

# Measuring the Neutral Pion Polarizability

## Letter of Intent Submitted to PAC 47

M.M. Ito<sup>1</sup>, J. Goity<sup>1,2</sup>, D. Lawrence<sup>1</sup>, E.S. Smith<sup>\*1</sup>, B. Zihlmann<sup>1</sup>, R. Miskimen<sup>3</sup>, I. Larin<sup>3</sup>, A. Aleksejevs<sup>4</sup>,  
S. Barkanova<sup>4</sup>, A. Austregesilo<sup>5</sup>, D. Hornidge<sup>6</sup>, and P. Martel<sup>7</sup>

<sup>1</sup>*Thomas Jefferson National Accelerator Facility, Newport News, VA*

<sup>2</sup>*Hampton University, Hampton, VA*

<sup>3</sup>*University of Massachusetts, Amherst, MA*

<sup>4</sup>*Memorial University of Newfoundland, Corner Brook, Canada*

<sup>5</sup>*Carnegie Mellon University, Pittsburgh, PA*

<sup>6</sup>*Mount Allison University, Sackville, New Brunswick, Canada*

<sup>7</sup>*Institute for Nuclear Physics, Johannes Gutenberg University, Mainz, Germany*

May 23, 2019

---

\*Contact Person, email: [elton@jlab.org](mailto:elton@jlab.org)

## Abstract

This proposal presents our plan to make a precision measurement of the cross section for  $\gamma\gamma \rightarrow \pi^0\pi^0$  via the Primakoff effect using the GlueX detector in Hall D. The aim is to significantly improve the data in the low  $\pi^0\pi^0$  invariant mass domain, which is essential for understanding the low energy regime of Compton scattering on the  $\pi^0$ . In particular, the aim is to obtain a first accurate experimental determination of the neutral pion polarizability  $\alpha_\pi - \beta_\pi$ , which is one of the important predictions of chiral perturbation theory and a key test of chiral dynamics on the  $\pi^0$ . Our goal is to measure  $\sigma(\gamma\gamma \rightarrow \pi^0\pi^0)$  to a precision of  $\sim 1\%$ , which would determine the combination of  $\alpha_{\pi^0} - \beta_{\pi^0}$  to a precision of 10%. We expect this experiment to run concurrently with the previously approved experiment to measure the charged pion polarizability (CPP) [1] in Hall D.

## 1 Introduction

Electromagnetic polarizabilities are fundamental properties of composite systems such as molecules, atoms, nuclei, and hadrons [2]. Whereas form factors provide information about the ground state properties of a system, polarizabilities provides information about the excited states of the system, and are therefore determined by the system's dynamics. Measurements of hadron polarizabilities provide an important test point for Chiral Perturbation Theory, dispersion relation approaches, and lattice calculations. Among the hadron polarizabilities, the neutral pion polarizability ranks of paramount importance because it tests fundamental symmetries, in particular chiral symmetry and its realization in QCD. Indeed, the non-trivial (non-perturbative) vacuum properties of QCD result in the phenomenon of spontaneous chiral symmetry breaking, giving rise to the Goldstone Boson nature of the pions. In particular, the Goldstone Boson nature of the  $\pi^0$  manifests itself most notably in its decay into  $\gamma\gamma$  and also in its electromagnetic polarizabilities, which according to ChPT can be predicted to leading order in the expansion in quark masses.

Hadron polarizabilities are best measured in Compton scattering experiments where, in the case of nucleon polarizabilities, one looks for a deviation of the cross section from the prediction of Compton scattering from a structureless Dirac particle.

In the case of pions, the long lifetime of the charged pion permits experiments of low energy Compton scattering using a beam of high energy pions scattering on atomic electrons. On the other hand, the short lifetime of the neutral pion requires an indirect study of low energy Compton scattering via measurements of the process  $\gamma\gamma \rightarrow \pi^0\pi^0$ , a method that can also be applied to the charged pion (CPP) and for which a proposal in Hall D is already approved [1].

This proposal presents a plan to make a precision measurement of the  $\gamma\gamma^* \rightarrow \pi^0\pi^0$  cross section using the GlueX detector in Hall D. The measurement is based on the Primakoff effect which allows one to access the low  $W_{\pi^0\pi^0}$  invariant mass regime with a small virtuality of the  $\gamma^*$  representing the Coulomb field of the target. The central aim of the measurement is to drastically improve the determination of the cross section in that domain, which is key for constraining the low energy Compton amplitude of the  $\pi^0$  and thus for extracting its polarizability. At present, the only accurate measurements exist for invariant masses of the two  $\pi^0$ s above 0.7 GeV, way above the threshold 0.27 GeV. The existing data at low energy were obtained in  $e^+e^- \rightarrow \pi^0\pi^0$  scattering in the early 1990's with the Crystal Ball detector at the DORIS-II storage ring at DESY [3].

Meanwhile, theory has made significant progress over time, with studies of higher chiral corrections ([4], [5], [6]) and with the implementation of dispersion theory analyses which serve to make use of the higher energy data [7, 8, 9, 10]. It is expected that the experimental data from this proposal, together with those theoretical frameworks, will allow for the most accurate extraction of the  $\pi^0$  polarizabilities to date.

## 2 Theoretical predictions for the neutral pion polarizability

The low energy properties of pions are sensitive to their nature as the Goldstone Bosons of spontaneously broken chiral symmetry in QCD, and are described in a model independent way by the framework of Chiral Perturbation Theory (ChPT) (Gasser and Leutwyler [11]), which implements a systematic expansion in low energy/momentum and in quark masses. In particular the pions' low energy electromagnetic properties can serve as tests of their Goldstone Boson (GB) nature. One such a case is the  $\pi^0 \rightarrow \gamma\gamma$  decay, which at the same time tests its GB nature and the chiral anomaly. Another case is low energy Compton scattering on pions: at low energy the Compton differential cross section can be expanded in powers of the photon energy and expressed in terms of the corresponding pion charge and the electric and magnetic polarizabilities, where the latter give the order  $\omega^2$  terms in the Compton cross section. The polarizabilities appear as deviations of the pions from point like particles, and thus result from carrying out the chiral expansion to the next-to-leading order. For both charged and neutral pions the polarizabilities are fully predicted at leading order in quark masses, and thus represent a sensitive test of chiral dynamics. For the charged pions, at  $O(p^4)$  ChPT predicts that the electric and magnetic polarizabilities ( $\alpha_{\pi^+}$  and  $\beta_{\pi^+}$ ) are related to the charged pion weak form factors  $F_V$  and  $F_A$  in the decay  $\pi^+ \rightarrow e^+\nu\gamma$

$$\alpha_{\pi^+} = -\beta_{\pi^+} \propto \frac{F_A}{F_V} = \frac{1}{6}(l_6 - l_5), \quad (1)$$

where  $l_5$  and  $l_6$  are low energy constants in the Gasser and Leutwyler effective Lagrangian [11]. Using recent results from the PIBETA collaboration for  $F_A$  and  $F_V$  [12], the  $O(p^4)$  ChPT prediction for the charged pion electric and magnetic polarizabilities is given by:

$$\alpha_{\pi^+} = -\beta_{\pi^+} = (2.78 \pm 0.1) \times 10^{-4} \text{ fm}^3. \quad (2)$$



Figure 1:

In the case of the neutral pion, the polarizabilities are determined by the one loop chiral contributions (see Fig. 1) which are calculable, free of unknown parameters, and given only in terms of the fine structure constant, the pion mass and the pion decay constant:

$$\begin{aligned} \alpha_{\pi^0} + \beta_{\pi^0} &= 0 \\ \alpha_{\pi^0} - \beta_{\pi^0} &= -\frac{\alpha}{48\pi^2 M_\pi F_\pi^2} \simeq -1.1 \times 10^{-4} \text{ fm}^3 \end{aligned} \quad (3)$$

However, there is a range of predictions beyond NLO and the experimental test of these important predictions is very challenging. In the first place, the polarizabilities drive the very low energy regime of Compton scattering on the  $\pi^0$  as there is no Thomson term, so one would expect that it would be easier to determine them than in the charged pion case. However, in the first place Compton scattering on the  $\pi^0$  is experimentally inaccessible due to its short lifetime, and therefore it is necessary to resort to the process of this proposal. In addition, ChPT indicates that the polarizabilities are smaller in the case of the neutral pion, about a third of their value for the charged pion, i.e. somewhere between  $-1.7 \times 10^{-4} \text{ fm}^3$  and  $-1.9 \times 10^{-4} \text{ fm}^3$ , depending on the model. The challenge is therefore to measure the cross section for  $\gamma\gamma \rightarrow \pi^0\pi^0$  with sufficient accuracy at low invariant mass  $W_{\pi\pi}$  so that one can infer the low-energy Compton amplitude and extract the polarizabilities. For this purpose, the theoretical foundations have been laid in works studying  $\gamma\gamma \rightarrow \pi^0\pi^0$  both using ChPT (Bellucci et al [13, 4], Gasser et al [5], Aleksejevs and Barkanova [6]) and dispersion theory (Oller and Roca [7], Dai and Pennington [8, 9], Moussallam [10]). In particular, in ChPT at the next-to-next to leading order, which provides the higher order quark mass corrections to the polarizabilities, some of the low energy constants need to be fixed and for that a significantly more accurate measurement of the  $\gamma\gamma \rightarrow \pi^0\pi^0$  cross section is needed than available presently.

Accurate measurements of the cross section near threshold combined with data for  $W_{\pi\pi} > 0.7$  GeV will provide the necessary input for performing a full theoretical analysis, combining dispersion theory with and without inputs from ChPT at low energy. This is a well established method which has been used to analyze  $\pi\pi$  scattering. Through such an analysis it will be possible to determine, via combination with ChPT, the low energy Compton amplitude and extract the polarizability combination  $\alpha_\pi - \beta_\pi$ . The latter extraction represents some challenge as shown in Fig. 2, where the polarizabilities have a small effect on  $W_{\pi\pi}$  below 0.5 GeV. Calculations by Dai and Pennington (Table II) [14] indicate that a 1.3% determination of  $\sigma(\gamma\gamma \rightarrow \pi^0\pi^0)$  will determine the combination of  $\alpha_{\pi^0} - \beta_{\pi^0}$  to a precision of 10%. The preliminary study done by Aleksejevs and Barkanova for this proposal in relativistic ChPT with SU(3) input indicate that sensitivity could be even better depending on specific kinematics; the full evaluation is in progress. In general, the determination of the accuracy one can get for  $\alpha_\pi - \beta_\pi$  based on a more accurate measurement as the one proposed here is still an issue to be further studied theoretically, with J. Goity and A. Aleksejevs forming a group to take a lead on the project. However, even 10% precision would still be sufficient to difference between various models and facilitate extraction of low-energy constants, and thus a highly desirable result for theory.

### 3 Past Measurements

Past measurements of the  $\gamma\gamma \rightarrow \pi^0\pi^0$  cross section can be summarized as follows:

1. In the early 1990's measurements were made in  $e^+e^-$  collisions at DESY with the XBall detector at the DORIS-II storage ring, which are the only available data for  $W_{\pi\pi} < 0.6$  GeV [3].
2. In 2008-9, measurements were carried out by BELLE for  $0.6 \text{ GeV} < W_{\pi\pi} < 4.0$  GeV [15, 16, 17].

Several works have made use of dispersion theory methods (Oller and Roca [7], Dai and Pennington [14], and in particular Moussallam [10] who performed the dispersive analysis where one of the photons has non vanishing virtuality, which is particularly important for our case.) with those available data. In particular these methods give results for the cross section at small  $W_{\pi\pi}$ , but the poor accuracy of the data in that region does not serve as a useful constraint that could improve those analyses. On the other hand, the ChPT calculations carried out at NNLO (Bellucci et al [13, 4] ) can only be fitted to the low  $W_{\pi\pi}$  data, and thus the uncertainty in the fixing of low energy constants is rather large. It is therefore expected that accurate data at low  $W_{\pi\pi} < 0.6$  GeV will have a very big impact on both theoretical approaches, which together may allow for an accurate description of the low energy Compton amplitude,

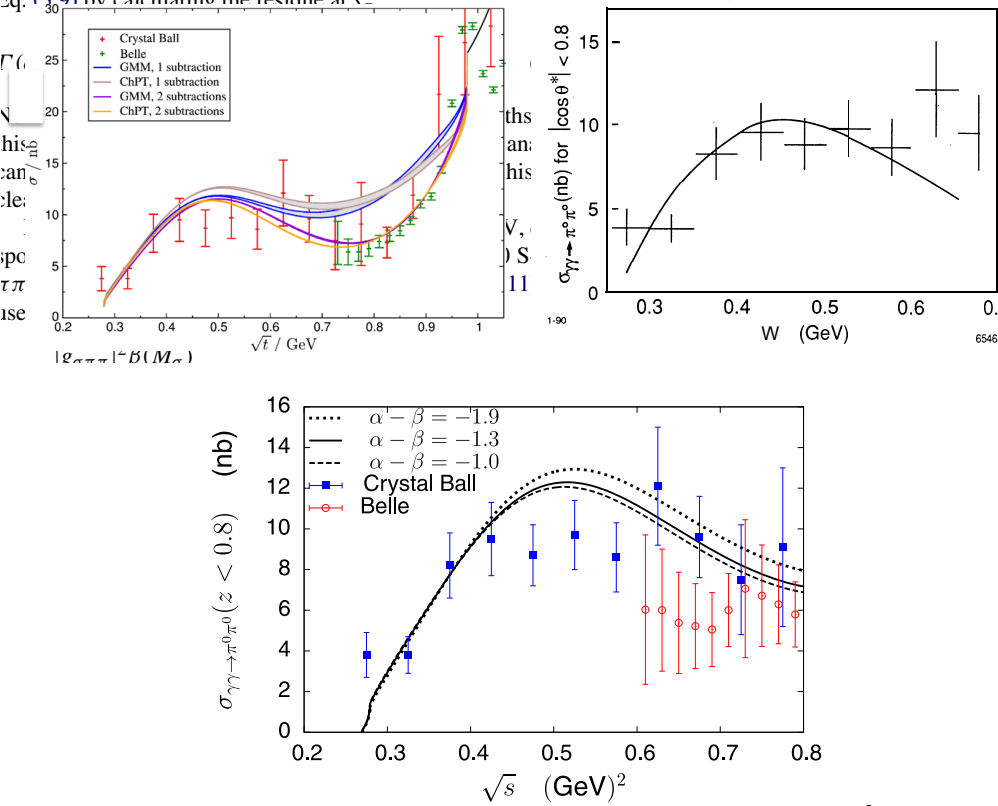


Figure 2: Left panel: experimental status; right panel: results from the 1990 XBall experiment. The lower panel shows the effect of  $\pi^0$  polarizabilities on the cross section ( $\sqrt{s} = W_{\pi\pi}$ ) [10].

and for a first time experimental determination of the polarizability.

## 4 Experimental conditions

The measurement of the neutral pion polarizability is expected to run concurrently with the experiment to measure the charged pion polarizability (CPP) [1] in Hall D. Essentially all the optimizations for that experiment are expected to improve the sensitivity of this experiment also. We briefly summarize the configuration for CPP, which is compared in Table 1 to nominal GlueX running.

The diamond radiator will be adjusted to set the coherent peak of the photon

Table 1: Configuration of the CPP experiment compared to nominal GlueX. This experiment is expected to run concurrently with CPP. Detectors not identified in the table are assumed to be operated under the same conditions as in the nominal configuration.

Configuration	Nominal GlueX	CPP
Electron beam energy	12 GeV	11.6 GeV
Emittance	$10^{-8}$ m rad	$10^{-8}$ m rad
Electron current	220 nA	20 nA
Radiator thickness	20 $\mu$ m	50 $\mu$ m diamond
Coherent peak	8.4 – 9.0 GeV	5.5 – 6.0 GeV
Collimator aperture	3.5 mm	5 mm
Peak polarization	44%	72%
Tagging ratio	0.56	0.72
Flux 5.5-6.0 GeV		11.7 MHz
Flux 0.3-11.3 GeV		74 MHz
Target position	65 cm	1 cm
Target, length	H, 30 cm	$^{208}$ Pb, 0.028 cm
Start counter	nominal	removed
Muon identification	None	Behind FCAL

beam between 5.5 and 6 GeV. This enhances the polarization significantly and also the tagging ratio. The experimental target will be placed upstream of the nominal GlueX target by 64 cm ( $z=1$  cm in the Hall D coordinate system). These changes benefit the present experiment. In addition, the CPP experiment will add multi-wire proportional chambers downstream for muon identification, but these do not impact this measurement one way or another.

## 4.1 Expected signal

In order to estimate rates, resolution and acceptance due to the Primakoff reaction on lead,  $\gamma^{208}\text{Pb} \rightarrow \pi^0\pi^0\text{Pb}$ , we take the reaction process to be the same as for charged pion production and given in Eq. 8 of the Proposal for the Charged Pion Polarizability experiment [1], which is reproduced here for convenience:

$$\frac{d^2\sigma}{d\Omega_{\pi\pi}dW_{\pi\pi}} = \frac{2\alpha Z^2 E_\gamma^4 \beta^2 \sin^2 \theta_{\pi\pi}}{\pi^2 W_{\pi\pi} Q^4} |F(Q^2)|^2 \sigma(\gamma\gamma \rightarrow \pi^0\pi^0) (1 + P_\gamma \cos 2\phi_{\pi\pi}). \quad (4)$$

The  $\gamma\gamma$  cross section for charged pions has been substituted with the cross section for neutral pions, namely  $\sigma(\gamma\gamma \rightarrow \pi^0\pi^0)$ . In this expression,  $\Omega_{\pi\pi}$  is the solid angle in the laboratory frame for the emission of the  $\pi\pi$  system,  $W_{\pi\pi}$  is the  $\pi\pi$  invariant mass,  $Z$  is the atomic number of the target,  $\beta$  is the velocity of the  $\pi\pi$  system,  $E_\gamma$  is the energy of the incident photon,  $F(Q^2)$  is the electromagnetic form factor for the target with final-state-interactions (FSI) corrections applied,  $\theta_{\pi\pi}$  is the lab angle for the  $\pi\pi$  system,  $\phi_{\pi\pi}$  is the azimuthal angle of the  $\pi\pi$  system relative to the incident photon polarization, and  $P_\gamma$  is the incident photon polarization.<sup>1</sup>

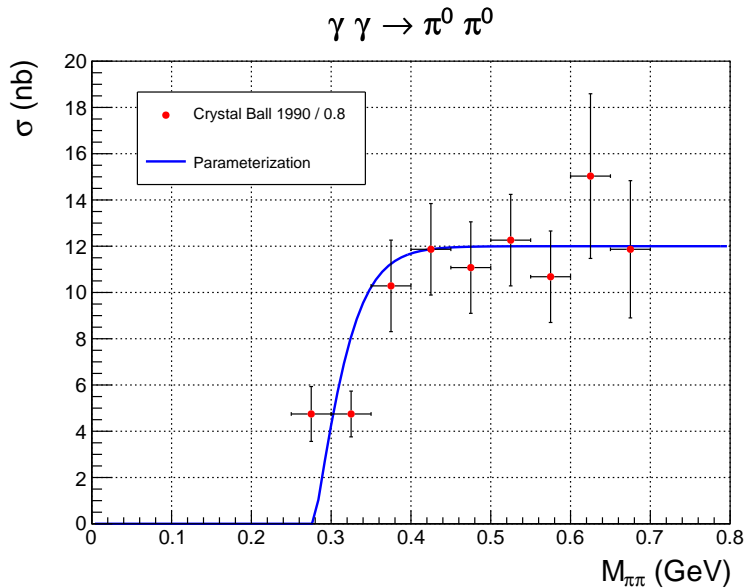


Figure 3: Parameterization of the  $\sigma(\gamma\gamma \rightarrow \pi^0\pi^0)$  cross section as a function of the  $2\pi$  invariant mass compared to the data from Crystal Ball [3].

The cross section for  $\sigma(\gamma\gamma \rightarrow \pi^0\pi^0)$  has been measured by the Crystal Ball Collaboration [3], albeit with limited statistical precision. We have parameterized the cross section for  $W_{\pi\pi} < 0.8$  GeV, which is of specific interest to this program as shown in Fig.3. Using this parameterization and Eq.4, we can calculate the photoproduction cross section on lead, which is shown in Fig.4. The integrated cross section is  $0.35 \mu\text{b}/\text{nucleus}$ . For reference, we note that the cross section for charged pions ( $\pi^+\pi^-$ ) production is  $10.9 \mu\text{b}$ , a factor of 30 larger.

The number of neutral-pion-Primakoff-signal events produced during 20 PAC days is shown in Fig.5. The impacts of detector trigger, acceptance and resolution are discussed in the next section.

<sup>1</sup>The expression for the cross section in terms of invariant quantities can be found in Ref. [18].

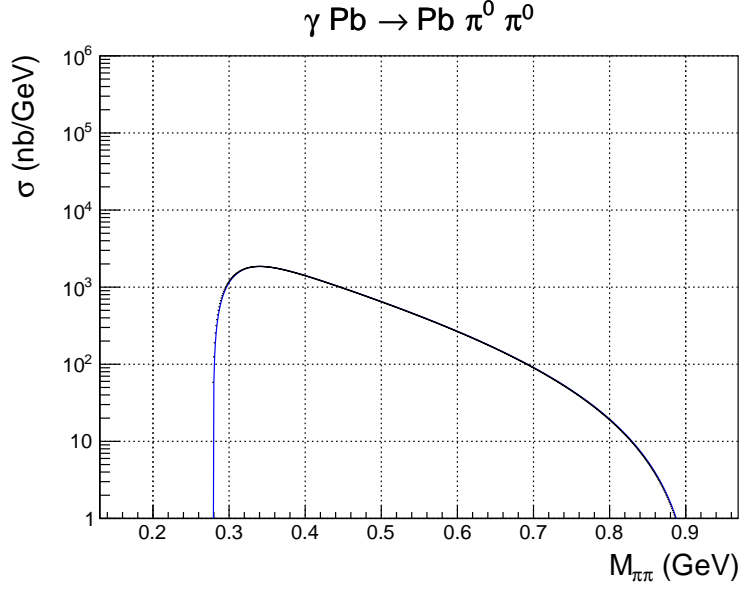


Figure 4: Primakoff cross section for  $\gamma Pb \rightarrow Pb \pi^0 \pi^0$  using the parameterization of  $\sigma(\gamma\gamma \rightarrow \pi^0 \pi^0)$  in the previous figure. The integrated cross section is  $0.35 \mu\text{b}/\text{nucleus}$ .

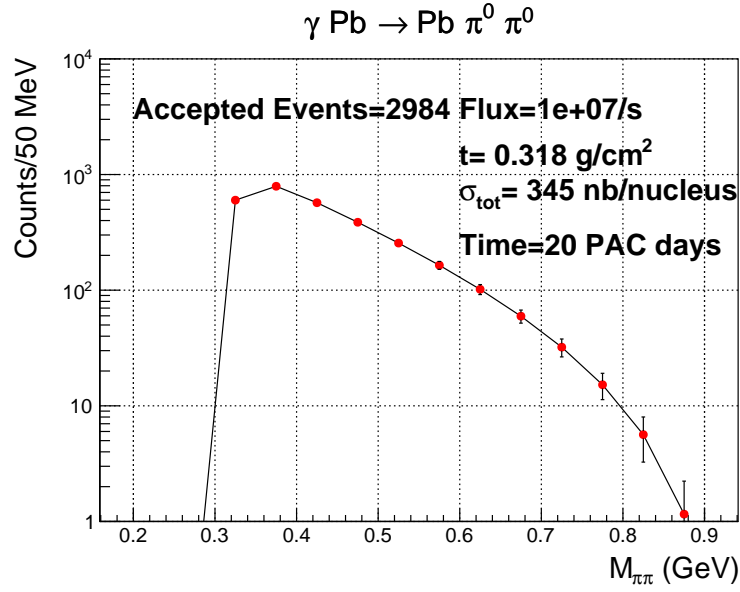


Figure 5: Estimated production rate for  $\gamma Pb \rightarrow \pi^0 \pi^0 Pb$  as a function of  $2\pi$  mass. For this calculation, it is assumed the detector has perfect resolution and has a linearly increasing efficiency from zero at threshold up to 0.6 at 0.34 GeV (see top right of Fig. 11 ).

## 4.2 Detector resolution

The response of the GlueX detector to neutral pion Primakoff events was simulated using the standard GlueX generation and reconstruction tools, but with the specific geometry for the CPP experiment. The schematic of the detector configuration is shown in Fig. 6. The primary differences between the standard GlueX geometry and CPP are summarized in Table 1. For this experiment, the main differences include a) coherent peak position at 5.5-6 GeV and re-positioning of the microscope to cover the coherent peak, b) solid  $^{208}\text{Pb}$  at  $z=1\text{cm}$ , and c) Start counter removed. For the CPP experiment, the addition of muon identification chambers behind the FCAL is critical. However, for neutral pions this addition plays no role because the photons are detected in the FCAL. The GEANT3 simulation, which is used for these studies, includes most changes except for the addition of the muon chambers, which are not needed. In addition, the microscope geometry has not been modified and we use the tagger hodoscope for that region in the simulation. The slightly reduced energy of the hodoscope relative to the microscope has little impact and the gaps between counters is ignored by simulating the tagged flux.

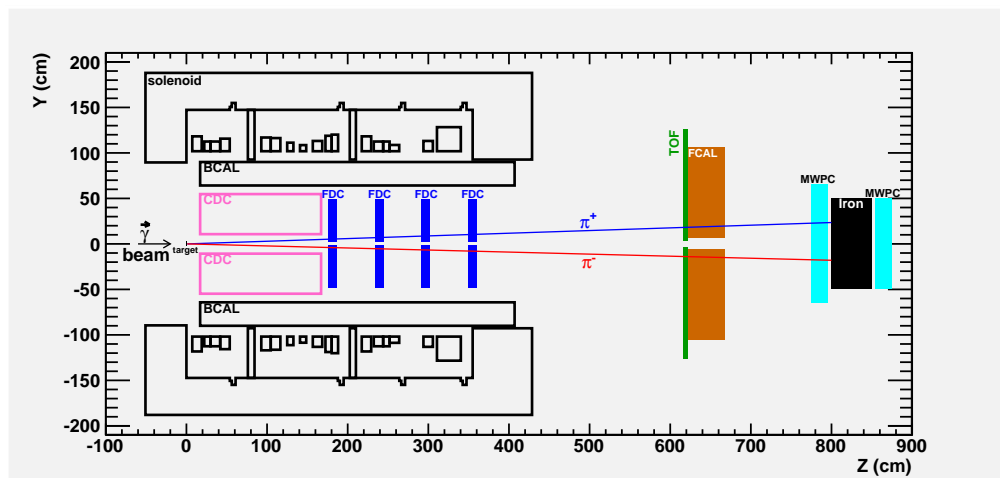


Figure 6: Diagram of the GlueX detector including the additional muon chambers for the CPP experiment.

The Primakoff signal was generated according to the cross section described in the previous chapter, using a modified version of the *gen\_2pi\_primakoff* event generator to generate  $\pi^0$ 's instead of charged pions. By default, the production amplitudes are symmetrized between the two identical  $\pi^0$ 's by AmpTools. One hundred thousand events were generated with  $M_{\pi\pi} < 0.5$  GeV and with no background, fed to GEANT3 to track particles, and subsequently processed using *mcsmeas* to simulate the detector response. The simulated events were then analyzed using the GlueX event filter to analyze the

reaction  $\gamma Pb \rightarrow \pi^0 \pi^0$  with a missing Pb nucleus and constraining the detected photon pairs to the  $\pi^0$  mass. The output of the reconstruction, both kinematically fit and “measured” quantities, were available for inspection.

In the following we show various reconstructed quantities as well as estimated resolutions. The distribution of generated photon energy and the unconstrained reconstructed momenta of the two pions are shown in Fig. 7. The missing mass,  $2\pi$  mass

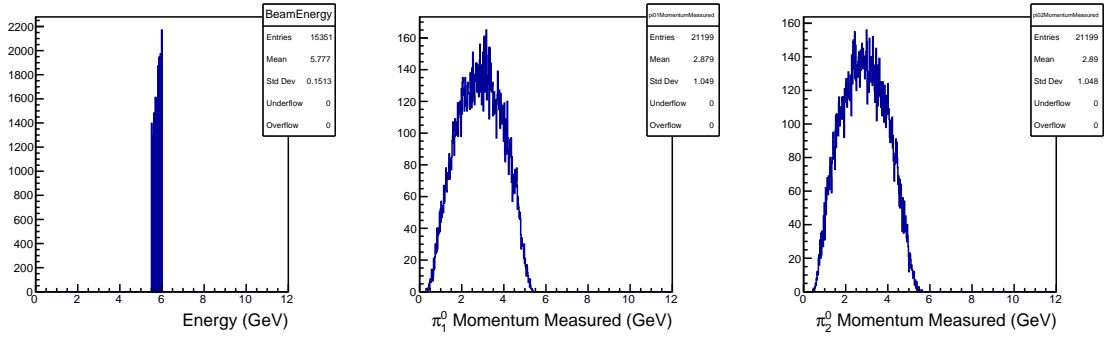


Figure 7: Left: Generated photon energies. Center: Reconstructed momentum distribution of one  $\pi^0$ . Right: Reconstructed momentum distribution of the second  $\pi^0$ .

and  $-t$  distributions are shown in Fig. 8. The reconstructed momentum relative to its

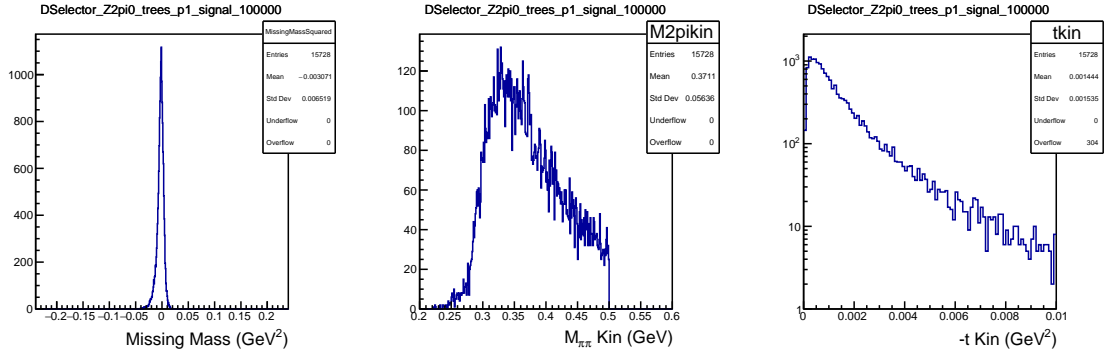


Figure 8: Left: Missing mass distribution minus the mass of the recoil nucleus. Center: Kinematically fit  $2\pi$  mass distribution. Right: Kinematically fit  $-t$  distribution.

generated value is shown in Fig.9. The central peak of the kinematicall fit momentum is about 2%, similar to that for charged pions. However, there are long uniform tails that will effect the final reconstruction. The resolution of the azimuthal angle,  $\phi_{\pi\pi}$ , between the production and the photon polarization planes is quite poor owing to the

fact that the pion pairs are produced at very shallow angles. Nevertheless it is sufficient to measure the asymmetry due to the photon beam polarization. The resolution of the

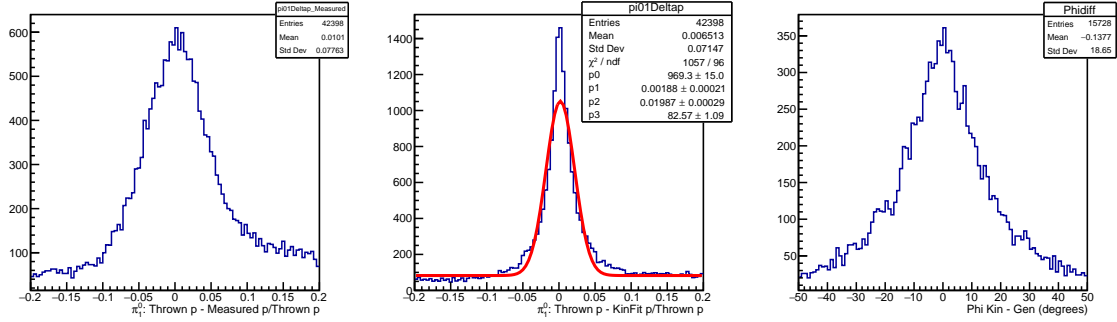


Figure 9: Left: Difference between measured and generated momentum. Center: Difference between kinematically fit and generated momentum. The central peak has a width of about 2%. Right: Difference between the kinematically fit azimuthal angle  $\phi_{\pi\pi}$  and its generated value.

$2\pi$  invariant mass is shown in Fig. 10, along with the resolution of Mandelstam  $-t$ , and the reconstructed time resolution. The mass resolution is about 8 MeV.

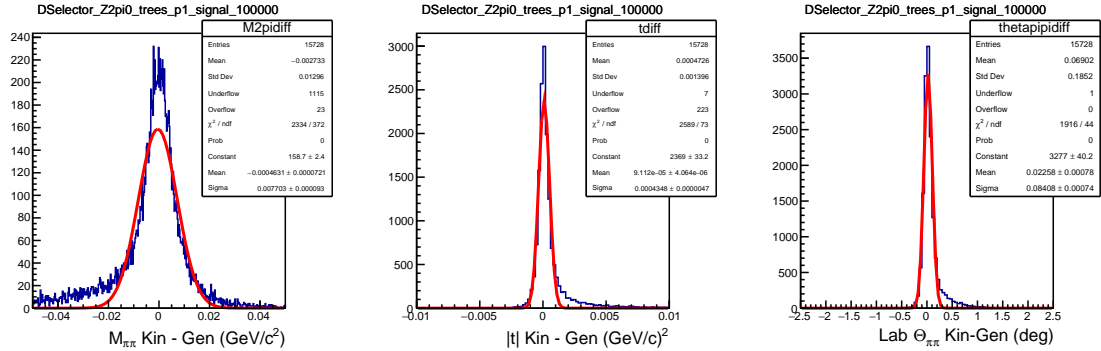


Figure 10: Left: Difference between kinematically fit and generated  $2\pi$  mass. The central  $2\pi$ -mass  $\sigma$  is about 8 MeV. Center: Difference between kinematically fit and generated  $-t$ . Right: Difference between kinematically fit and generated  $2\pi$  polar angle. The resolution  $\sigma$  of the reconstructed angle is less than 0.1 degrees.

### 4.3 Trigger and acceptance

The Primakoff reaction will transfer all the energy of the beam into four photons, which are going forward. All this energy will be deposited in the FCAL, except for leakage down the beampipe. We expect a simple trigger with an energy threshold in the FCAL should have very high efficiency for any events that can be reconstructed.

The acceptance of the signal events can be determined by comparing the kinematically fit to the generated distributions. The generated and kinematically fit  $2\pi$  mass,  $\phi_{\pi\pi}$  and  $-t$  distributions are shown in Fig. 11. The reconstruction was described in the previous section. The acceptance is quite high at about 60%. However, there is also significant slewing due to resolution in most variables of interest. The main effect of resolution in the  $2\pi$  mass happens at threshold and the distortions above that are not very great. The relatively poor resolution in  $\phi_{\pi\pi}$  results in dilution of the measured azimuthal dependence, which will need to be adjusted based on simulation. Finally the  $-t$  resolution softens the measured  $t$ -slope due to the smearing of high rate regions down to low rate regions.

### 4.4 Backgrounds

#### 4.4.1 Coherent and incoherent backgrounds in the reaction

Coherent  $\rho^0$  photo-production is not a background for this experiment because  $\rho^0$  decay into the  $\pi^0\pi^0$  channel is prohibited by I-spin conservation. The largest coherent background is from  $f_0(500)$  and  $f_0(980)$  photo-production. The width of the  $f_0(980)$  is from 10 to 100 MeV, and can be eliminated from the data by a cut on  $\pi^0\pi^0$  invariant mass. The  $f_0(500)$  width is much broader, from 400 to 700 MeV, with significant overlap in the invariant mass region of interest. Since the  $f_0(500)$  is a scalar particle with the same spin-parity as the  $\gamma\gamma \rightarrow \pi^0\pi^0$  final state near threshold, the azimuthal distribution of the  $\pi^0$  momentum or the  $\pi^0\pi^0$  c.m. momentum relative to the photon polarization plane does not differentiate between coherent  $f_0(500)$  production and the Primakoff reaction. This is similar to the Primex- $\pi^0$  experiment, where the dominant background was nuclear coherent  $\pi^0$  photo-production. The approach used in the Primex analysis was to measure the  $\pi^0$  angular distribution, effectively the  $t$ -distribution, then use theoretical calculations of the angular distributions to separate out contributions from Primakoff and nuclear coherent. The analysis of the  $\pi^0\pi^0$  (NPP) reaction will approximately parallel what was done for the Primex- $\pi^0$  analysis.

Primex data also showed that the nuclear coherent process is highly suppressed for heavy nuclei. The reason for the suppression is  $\pi^0$  absorption in the nuclear interior, making the coherent production primarily a surface effect, i.e. proportional to  $A$  and not  $A^2$ . For NPP it is expected that suppression of the nuclear coherent will be stronger

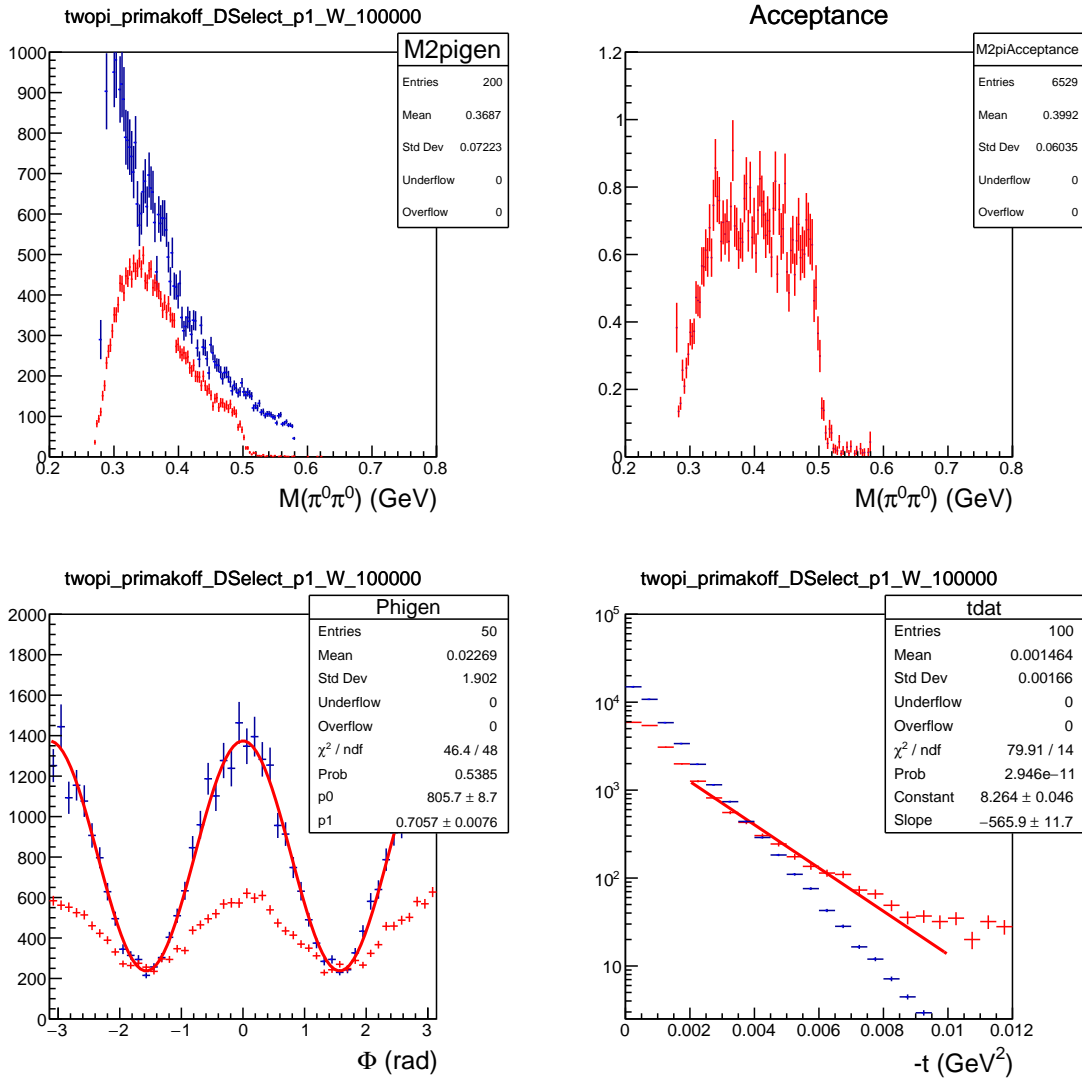


Figure 11: Top left: Generated and kinematically fit  $2\pi$  mass distribution. Top right: Acceptance as a function of  $2\pi$  mass. Events above  $M_{\pi\pi} > 0.5$  GeV were eliminated from the analysis. The acceptance is about 60%. Bottom left: Generated and kinematically fit azimuthal angle  $\phi_{\pi\pi}$ . Bottom right: Generated and kinematically fit  $-t$  distribution. There is significant slewing of the measured distribution to large  $-t$ .

than that seen in Primex because two pions are produced in NPP as compared to a single  $\pi^0$  in Primex. NPP plans to run on a heavy nuclear target such as  $^{208}\text{Pb}$ .

The inelastic and incoherent reactions that might contribute to the data include

- (i) nuclear coherent production of  $\eta$  followed by  $\eta \rightarrow \pi^0\pi^0\pi^0 \rightarrow \gamma\gamma\gamma(\gamma\gamma)$ , where two of the six decay photons go unobserved
- (ii)  $\gamma N \rightarrow N\pi^0\pi^0$

The first reaction is an inelastic, coherent process, and as such could produce a significant rate for a heavy nuclear target. Rejecting events with extra gammas in the final state would suppress this background. The second reaction is an incoherent process, and is small relative to coherent processes. The Primex analysis showed that incoherent reactions generally peak at large angles relative to the Primakoff peak, and had a small effect on the extraction of the Primakoff  $\pi^0$  cross sections.

#### 4.4.2 Analysis of existing data

We investigated the challenges of reconstructing  $2\pi^0$  final states with a missing recoil proton using the 2017 GlueX data taken with a Hydrogen target.<sup>2</sup> We selected and reconstructed events that matched the topology of the reaction  $\gamma p \rightarrow \gamma\gamma\gamma(p)$  with a missing proton. A kinematic fit was performed that conserved energy and momentum and imposed a vertex constraint at  $z=65$  cm ( $\text{CL} > 10^{-6}$ ). We note that even though the vertex was fixed at 65 cm to perform the fit, the actual target extends from 50 to 80 cm. Several other nominal selections were imposed to clean up the event sample, including no charged tracks and no missing energy. No constraints were imposed on the  $\pi^0$  mass in order to study backgrounds. Accidental background subtractions were performed to obtain the resulting mass distributions.

The invariant mass distributions of two photon pairs each show a strong  $\pi^0$  peak, as shown in the top of Fig. 12. There are background events that fall under the two  $\pi^0$  peaks, which requires further study, nevertheless, using the selection of photon pairs that reconstruct to the  $\pi^0$ , we can plot the  $2\pi^0$  mass spectrum (bottom of Fig. 12). The mass spectrum has recognizable features, in particular the prominent  $f_2(1270)$  that decays to  $\pi^0\pi^0$  85% of the time. The structure at  $M_{\pi\pi} \sim 0.8$  GeV appears too low for the  $f_0(980)$  and is present in a location where the Crystal Ball data [3] shows a low yield. The yield for  $M_{\pi\pi} < 0.5$  GeV is consistent within a factor of two of the relative yield compared to the  $f_2(1270)$  peak in the Crystal Ball data. This analysis demonstrates that these neutral events can be analyzed in our detector under significant more challenging circumstances than we anticipate for the Primakoff experiment. In

---

<sup>2</sup>GlueX has not taken any data with a nuclear target.

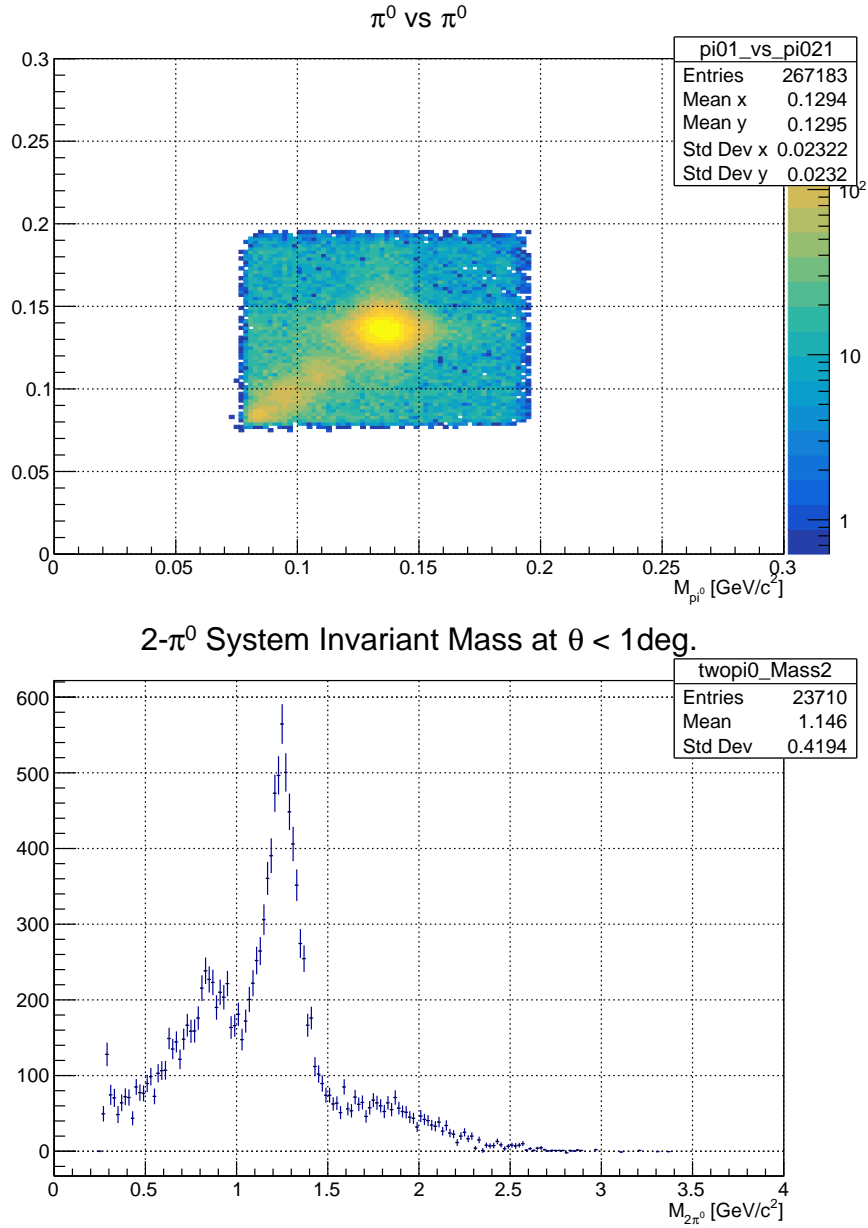


Figure 12: Experimental distributions from the 2017 GlueX data set analyzed as  $\gamma p \rightarrow \gamma\gamma\gamma(p)$  with a missing proton. Top: Two photon invariant mass of one pair vs the two photon invariant mass of the second pair. Bottom:  $2\pi$  mass distribution selecting events with the reconstructed photon pair masses close to the  $\pi^0$  mass as shown above. The plot also requires that the angle of the two pion system be less than 1 degree.

particular, for the Primakoff experiment, we will have a point nuclear target that will allow valid geometrical constraints and limit the amount of missing momentum in the reaction. This will make the kinematic fitting more effective.

It is evident from top plot in fig. 12 that a cut on the invariant mass of one reconstructed  $\pi^0$  will reduce the background on the other  $\pi^0$  significantly. This is shown in fig. 13 where a cut on the invariant of one  $\pi^0$  significantly reduces the background in the other while keeping the main signal mostly undisturbed.

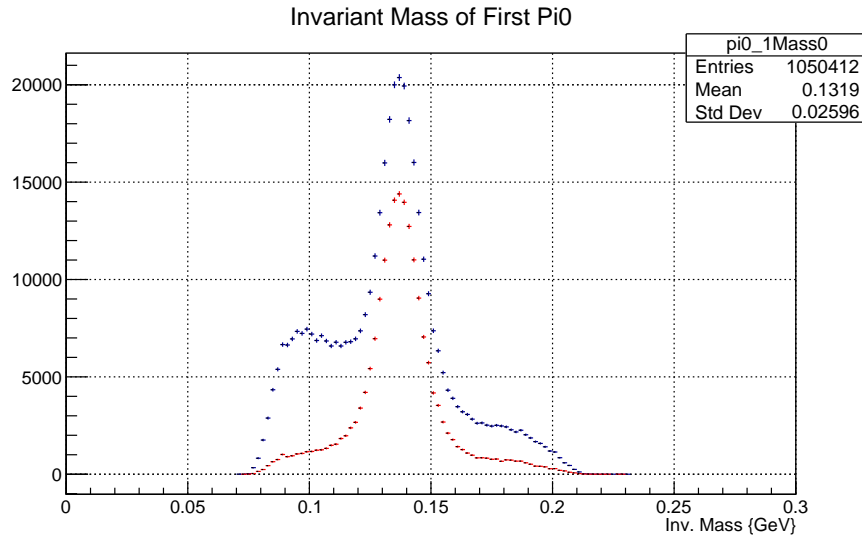


Figure 13: Invariant mass of the two photon system with (red) and without (blue) a cut on the invariant mass of the second pair of photons.

These photons are detected by the lead-glass calorimeter and are the main contribution to the resolution of the reconstructed  $\pi^0$  mass. A lead-tungstate calorimeter with a substantially better energy resolution would yield a significant improvement in the signal to noise ratio as the width of the reconstructed  $\pi^0$  would be smaller by about a factor of 2.

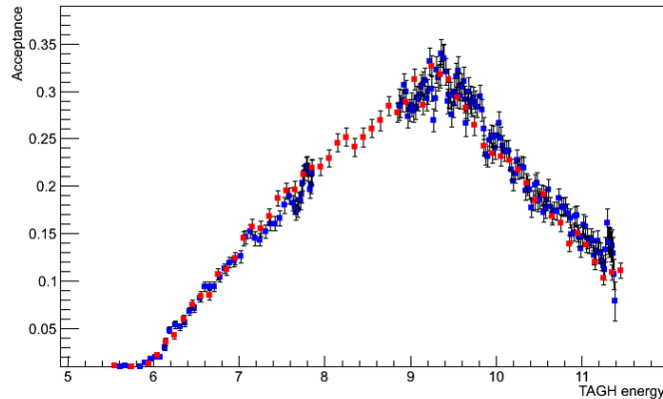


Figure 14: GlueX PS acceptance extracted from TAC data analysis (blue points); red points – Monte-Carlo simulation

## 5 Photon beam flux

### 5.1 Photon beam flux accounting with the GlueX pair spectrometer

The photon beam flux can be directly extracted by analyzing the pair spectrometer (PS) data with the thin beryllium converter installed in the beam in front of it. The absolute normalization of the PS performed with the total absorption counter (TAC) during the dedicated run.

The systematics from the photon beam flux accounting by pair spectrometer is originated from few main contributions: overall spectrometer calibration with TAC quality; accuracy of the Monte-Carlo simulation of this process; long term stability of the spectrometer performance; and change of conditions between low intensity beam (TAC calibration) and production intensity. There are few other less significant contributions. GlueX PS acceptance [19] shown on Fig. 14. For the proposed experiment PS magnetic field should be reduced to cover the beam energy range  $5 - 6 \text{ GeV}$ . The methodology and accuracy of the PS analysis is the same as in PrimEx-D experiment, currently running in Hall-D, and has value  $\sim 1 - 1.5 \%$  [20].

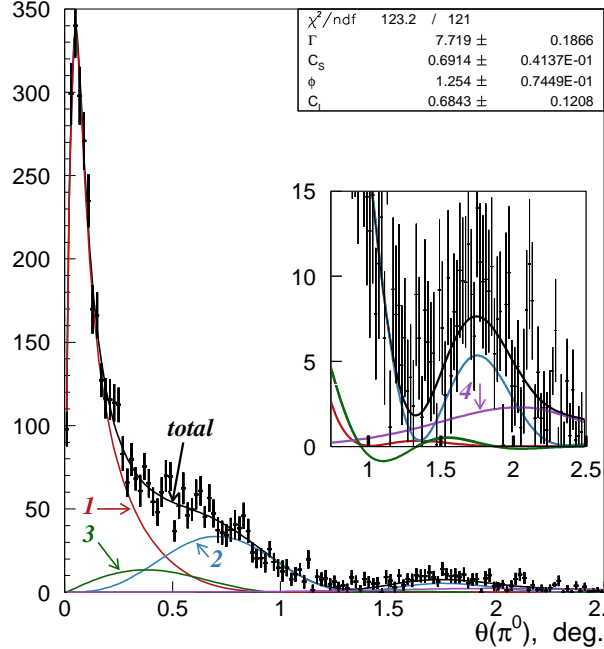


Figure 15: Exclusive  $\pi^0$  production yield at forward angle on lead target observed in the PrimEx experiment [21]. Curves show production mechanisms input: 1 – Primakoff, 2 – strong coherent, 3 – interference of first two mechanisms, 4 – strong incoherent

## 5.2 Cross section verification with the exclusive single $\pi^0$ photoproduction

The extracted cross section can also be normalized on or independently from PS analysis verified with the  $\pi^0$  radiative decay width extraction. Fig. 15 shows exclusive single  $\pi^0$  photoproduction yield at forward angle obtained by the PrimEx experiment and used for  $\pi^0$  radiative decay width extraction. The photon beam flux in PrimEx was  $0.725 \times 10^{12}$  for 4.9-5.5 GeV bremsstrahlung spectrum part on 5% rad. len. lead target. The distance between calorimeter and target was  $\sim 7.3 m$  and the central square part of the calorimeter, used in analysis was  $\sim 70 \times 70 cm$ . These conditions have to be compared with the proposed experiment conditions: 20 days of  $10^7$  collimated beam photon/sec (i.e. 20 times more than PrimEx lead target beam flux), the distance between target and FCAL  $\sim 6.2 m$  and active calorimeter part diameter  $\sim 2 m$ . The central hole with one calorimeter modules layer around which should be excluded from the analysis for PrimEx case was  $\sim 8 \times 8 cm$  and for FCAL  $\sim 20 \times 20 cm$ , which is decreasing FCAL acceptance at forward angle. Comparison of these experimental conditions allows us expecting an order of magnitude higher exclusive single  $\pi^0$  pho-

toproduction statistics. Thus PrimEx statistical uncertainty for lead will be decreased from  $\sim 2.5\%$  down to  $\sim 1\%$ . For the systematical uncertainty, in PrimEx it was  $\sim 2.1\%$  and has two major contributions: yield extraction ( $\sim 1.6\%$ ) and photon beam flux accounting ( $\sim 1.0\%$ ). The first contribution is partly statistically driven and reduces with increasing of statistics; and the second one cancels out since it is the same photon beam flux for the single and double exclusive  $\pi^0$  photoproduction. The main factors increasing systematics for the proposed experiment are: the angular resolution of FCAL is about a factor of two worse than for PWO crystals used in the PrimEx analysis; and the magnetic field is not swiping out charged background like it was in PrimEx. As a result we can expect slightly worse systematical uncertainty than in PrimEx and statistical precision of  $\sim 1\%$ , i.e. total error  $2.5 - 3.5\%$  for  $\pi^0$  radiative width extraction (excluding absolute photon beam flux accounting, target number of atoms and partly FCAL trigger efficiency contributions to the systematics which are canceling out). The expected total beam flux uncertainty for such a normalization should also include the PrimEx total error of the  $\pi^0$  radiative width, which was recently reported as  $1.5\%$  [22]. All this gives  $\sim 3 - 4\%$  error for photon beam flux from normalization to the re-extracted  $\pi^0$  radiative decay width.

### 5.3 Muon pair production

In addition to these normalization channels, production of muon pairs, which has a known cross section, can be used as a measurement of photon flux. Since the experiment will be running concurrently with the Charged Pion Polarizability (CPP) experiment, the photon flux on target will be the same by definition. CPP plans to use muon pair creation by beam photons as its main normalization channel, and so those measurements will be available for normalization of the neutral pion channel as well. In the case of CPP, the GlueX track finding and fitting efficiency will have to be determined for muon pairs, but any systematic error in that determination will largely cancel when applied to charged pion pairs. That will not be the case for the neutral pion channel and will have to be taken into account when evaluating systematic errors due to this method of normalization. In any case, muon pair production should provide a useful check on the other methods mentioned above.

## 6 Summary

We have investigated the possibility of determining the neutral pion polarizabilities  $\alpha_{\pi^0} - \beta_{\pi^0}$  by making a measurement of the cross section of the Primakoff reaction  $\gamma\text{Pb} \rightarrow \pi^0\pi^0\text{Pb}$ . We propose to make this measurement using data taken simultaneously with the CPP[1] experiment in Hall D. The existing GlueX detector has sufficient

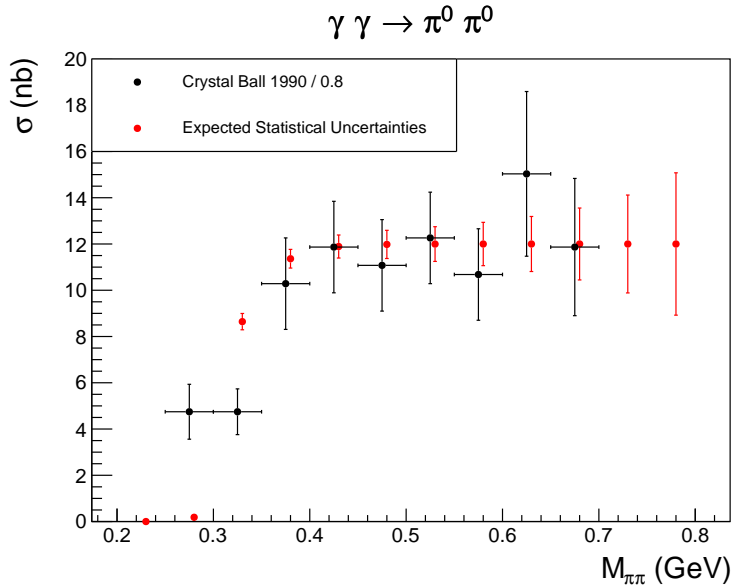


Figure 16: Estimated statistical uncertainties on determining  $\sigma(\gamma\gamma \rightarrow \pi^0\pi^0)$  in the absence of background during 20 PAC days running simultaneously with the approved CPP experiment. The data points from the single previous measurement are shown for comparison.

resolution and high acceptance for this process. We expect to collect approximately 3000 signal events during the approved 20 PAC days. The anticipated statistical uncertainties on the signal represent a significant improvement over existing data as shown in Fig. 16.

The current estimate by Dai and Pennington [14] indicates that a 1.3% determination of  $\sigma(\gamma\gamma \rightarrow \pi^0\pi^0)$  will determine the combination  $\alpha_{\pi^0} - \beta_{\pi^0}$  to a precision of 10%, but this estimate may be improved in the future with more kinematic-specific analysis. The theoretical work to model and to understand the backgrounds, such as hadronic  $t$ -exchange involving  $\rho^0$  and  $\omega$ , is ongoing.

## References

- [1] JLAB Experiment E12-13-008. Measuring the Charged Pion Polarizability in the  $\gamma\gamma \rightarrow \pi^+\pi^-$  Reaction, 2013. <https://misportal.jlab.org/mis/physics/experiments/viewProposal.cfm?paperId=789>.
- [2] Barry R. Holstein. Pion polarizability and chiral symmetry. *Comments Nucl. Part. Phys.*, 19(5):221–238, 1990.
- [3] H. Marsiske et al. A Measurement of  $\pi^0\pi^0$  Production in Two Photon Collisions. *Phys. Rev.*, D41:3324, 1990.
- [4] S. Bellucci, J. Gasser, and M. E. Sainio. Low-energy photon-photon collisions to two loop order. *Nucl. Phys.*, B423:80–122, 1994. [Erratum: *Nucl. Phys.*B431,413(1994)].
- [5] Juerg Gasser, Mikhail A. Ivanov, and Mikko E. Sainio. Low-energy photon-photon collisions to two loops revisited. *Nucl. Phys.*, ib728:31–54, 2005.
- [6] A. Aleksejevs and S. Barkanova. Electromagnetic Polarizabilities of Mesons. *Nucl. Part. Phys. Proc.*, 273-275:2773–2776, 2016.
- [7] J. A. Oller and L. Roca. Two photons into pi0 pi0. *Eur. Phys. J.*, A37:15–32, 2008.
- [8] Ling-Yun Dai and Michael R. Pennington. Comprehensive amplitude analysis of  $\gamma\gamma \rightarrow \pi^+\pi^-, \pi^0\pi^0$  and  $\bar{K}K$  below 1.5 GeV. *Phys. Rev.*, D90(3):036004, 2014.
- [9] Ling-Yun Dai and M. R. Pennington. Two photon couplings of the lightest isoscalars from BELLE data. *Phys. Lett.*, B736:11–15, 2014.
- [10] B. Moussallam. Unified dispersive approach to real and virtual photon-photon scattering at low energy. *Eur. Phys. J.*, C73:2539, 2013.
- [11] J. Gasser and H. Leutwyler. Chiral Perturbation Theory to One Loop. *Annals Phys.*, 158:142, 1984.
- [12] M. Bychkov et al. New Precise Measurement of the Pion Weak Form Factors in  $\pi^+ \rightarrow e^+ \nu_e \gamma$  Decay. *Phys. Rev. Lett.*, 103:051802, 2009.
- [13] S. Bellucci. Pion (kaon) and sigma polarizabilities. In *Chiral dynamics: Theory and experiment. Proceedings, Workshop, Cambridge, USA, July 25-29, 1994*, pages 177–189, 1994.
- [14] Ling-Yun Dai and Michael R. Pennington. Pion polarizabilities from  $\gamma\gamma \rightarrow \pi\pi$  analysis. *Phys. Rev.*, D94(11):116021, 2016.
- [15] T. Mori et al. High statistics measurement of the cross-sections of gamma gamma  $\rightarrow \pi^+\pi^-$  production. *J. Phys. Soc. Jap.*, 76:074102, 2007.
- [16] S. Uehara et al. High-statistics measurement of neutral pion-pair production in two-photon collisions. *Phys. Rev.*, D78:052004, 2008.

- [17] S. Uehara et al. High-statistics study of neutral-pion pair production in two-photon collisions. *Phys. Rev.*, D79:052009, 2009.
- [18] E.S. Smith. Calculation of the Primakoff cross section for  $\pi^+\pi^-$ . Technical Report GlueX-doc-**3186**, Jefferson Lab, January 2017. <https://halldweb.jlab.org/doc-private/DocDB/ShowDocument?docid=3186>.
- [19] A. Somov. Status of the Beam Flux Normalization from TAC runs. Technical Report GlueX-doc-**3684**, Jefferson Lab, February 2018. <https://halldweb.jlab.org/doc-private/DocDB/ShowDocument?docid=3684>.
- [20] JLAB Experiment E12-10-011. A Precision Measurement of the eta Radiative decay Width via the Primakoff Effect, 2010. <https://misportal.jlab.org/mis/physics/experiments/viewProposal.cfm?paperId=631>.
- [21] I. Larin et al. A New Measurement of the  $\pi^0$  Radiative Decay Width. *Phys. Rev. Lett.*, 106:162303, 2011.
- [22] I. Larin.  $\pi^0 \rightarrow \gamma\gamma$  Decay width: Final result from the PrimEx Collaboration, Oct 2018. DNP Meeting.